Polymer 254 (2022) 125039

Contents lists available at ScienceDirect

Polymer

journal homepage: www.elsevier.com/locate/polymer

Hierarchical solid-state structure and mechanical property relationships in cross-rolled polyethylene

N. McMullen *, C. Zhang, C. Cheng, G.E. Wnek, A. Olah, E. Baer

Department of Macromolecular Science and Engineering, Case Western Reserve University, Cleveland, OH, 44106, USA

ARTICLE INFO

Keywords:
Polyethylene
Deformation
Cold rolling
Hierarchical structure
Dynamic mechanical analysis

ABSTRACT

Deformation of polyethylene by bidirectional cold rolling was investigated. The objective was to better understand the evolution of the hierarchical structure with thickness reduction and the effect on mechanical properties. At a 60% thickness reduction, the thickness recovery after rolling peaked, and the density and crystallinity decreased rapidly resulting in greater optical clarity. Tensile specimens were deformed in uniaxial tension, and it was observed that the yield mechanism shifted from necking and whitening to a diffuse yielding process with extent of rolling. Concomitant greater work hardening, fracture stress, and elastic recovery were also observed upon fracture at both 25 °C and −40 °C. Scanning electron micrographs of the fracture surface revealed discrete buckled microlayers. Furthermore, dynamic mechanical analysis (DMA) revealed the loss tangent peaks associated with the beta and alpha relaxations shifted, suggesting that dilatation rather than compaction was the dominant mode of deformation at 60% thickness reduction.

1. Introduction

Deformation processing methods used in the post-processing of ductile metals have been employed commercially for centuries to form dimensionally uniform strips. Roll milling is one such process that has been ubiquitously adopted in the steel industry due to its suitability for continuous production [1,2]. Furthermore, roll milling offers a convenient way to enhance the mechanical properties of ductile metals. Rolling induced cold work in austenitic steels for instance enhances both the yield stress and ultimate tensile strength. Higher strengths in rolled steels are attributable structurally to grain refinement and increased dislocation density [3]. Deformation processing by cold roll milling has similarly been explored for semicrystalline polymeric materials as a means of molecular orientation by shear and compression. Cold roll milling takes place under room temperature conditions utilizing unheated rollers. For polyethylene, the material is deformed under heavy shear and compression between the glass transition and melting temperature. In comparison to orientation induced by extensional and shear flow in traditional processing methods for viscoelastic materials above the softening temperature, greater orientation can be retained in solid-state post-processing, as the chain orientation is frozen in place [4,5]. Such orientation is critical to improving the tensile strength of an initially isotropic polymeric material at the expense of increasing anisotropy and creating a weak direction.

Methods for the cold orientation of polymers in compression and shear have long been studied, including solid state extrusion [6], drawing through a channel die or mandrel [7], cold rolling [4–9], equal-channel angular extrusion and multi-angular extrusion (ECAE and ECMAE respectively), and high pressure torsion (HPT) [10]. Unlike methods such as solid-state drawing in pure uniaxial tension, which induces cavitation due to the presence of a dilatational stress condition, compressive stress states have been shown to suppress the nucleation of cavities which act as bulk defects (stress risers) that limit the elongation to failure in glassy polymers due to intense strain localization. Such high degrees of strain localization in turn prevent polymeric materials' application to drawing and forming operations requiring large elongations and high strain rates [7,11]. In crystalline polymers deformed under a dilatational stress condition, cavities have a tendency to nucleate in the amorphous interlamellar regions. Therefore, stress risers are similarly suppressed in the compressive deformation of crystalline polymers and the evolution of isotropic spherulites into a microfibrillar texture proceeds without microcavitation [7]. Instead, under a stress condition of compression and shear (such as in cold rolling), deformation proceeds by first forming isotropic spherulites into ones with oblong boundaries, and subsequently breaking up and tilting the crystalline lamellae at some critical thickness reduction to form a microfibrillar

* Corresponding author.
E-mail address: nam77@case.edu (N. McMullen).

https://doi.org/10.1016/j.polymer.2022.125039
Received 23 March 2022; Received in revised form 19 May 2022; Accepted 4 June 2022
Available online 13 June 2022

biaxial texture with a tight amorphous network [8]. Macroscopically, this change in mechanical behavior is observed in the yield process: in the absence of compression, the material responds to the applied stress by whitening and necking. On the other hand, the material exhibits diffuse yield behavior in the presence of a compressive stress state [7]. As with glassy polymers, isotropic crystalline polymeric materials cannot easily be processed using cold forming operations, especially ones with high strain rates and volumetric draw ratios. Because the polar and equatorial lamellar crystals deform by transverse slip vs. chain slip depending on their orientation relative to local stresses, the lamellae aligned with the direction of locally applied strain concentrate stresses during the deformation of isotropic spherulites resulting in strain localization [5]. Because the ability to delocalize strain relates to a material's capacity to dissipate energy by plastic deformation before failure [12], the evolution of a biaxial microfibrillar texture in crystalline polymers hold even further potential to improve the formability or drawability in a secondary processing step.

Previous work has connected the improvement in toughness to the shape of the damage zone and craze structure evolved in it. Snyder et al. [13] observed drastic improvement in the low temperature ductility of polypropylene after cross-rolling. Remarkably, this improvement in ductility takes place below the ductile-to-brittle transition temperature (DBT). In the unoriented material, the damage zone geometry was sharp (wedge shaped) resulting in a rapid fracture process at low temperatures. However, after cross-rolling a circular damage zone was formed during loading with penny-shaped delamination (c.f. fibrillar) crazes emanating from it in all directions. It was through this process that separation of the material along the plane of rolling took place. Furthermore, Osawa et al. [14] observed layered features on the fracture surface of compressively oriented iPP and suggested that these were spherulites that had been affinely deformed during compressive deformation and essentially flattened into "pancakes." However, the authors note that similar layered features are present in non-crystalline polystyrene as well. This work ultimately attributed the improvement in impact toughness at large compressive draws to delamination along the thickness direction resulting from orientation.

While delamination presents a mechanism for the dissipation of energy at larger strains when the damage zone becomes prominent, mesoscale and nanoscale damage mechanisms are critical to toughness at small and intermediate strains. On the microscale, crazing is associated with intense strain localization and softening [15]. On the other hand, shear banding, a form of continuum deformation (delocalized strain), is associated with greater work hardening and less softening at the yield point than crazing [12]. Classically, the ductile-to-brittle transition in polymeric materials is connected to the relaxation speed of amorphous chain segments which governs the micromechanism of irreversible damage (i.e. crazing vs. shear banding) which in turn governs brittle vs. ductile stress response. On the other hand, in crystalline polymers the supramolecular structure has been connected to the mechanical performance. The difference in strain response between polar and equatorial crystals is driven by the difference in stress required to activate crystal plasticity (i.e. yield stress. The difference in yield stress is in turn due to the differing energy requirements for the initiation of chain vs. transverse slip. The result is stress concentration on the supramolecular scale which induces strain localization [5].

Previously, hierarchical structure-mechanical property relationships have been elucidated for highly deformed crystalline polymers under compressive conditions. As with cold drawing in tension and simple shear, crystallographic mechanisms are responsible mechanistically for the deformation of the crystalline phase in a compressive stress condition, with chain slip seen as a dominant mechanism [16–19]. At relatively small strains, extension of the amorphous phase during interlamellar slip as well as chain slip accommodate the majority of the deformation. A large fraction of this deformation is reversible, with chain slip exhibiting complete reversibility [20]. At large strains, the capacity for the material to accommodate deformation through reversible slip processes is exhausted, and chain disentanglement leads to fully irrecoverable deformation [21]. Furthermore, a discontinuous lamellar fragmentation process is known to occur at sufficiently large strains and local shear stresses [18]. Given the complex and multifaceted damage mechanism for crystalline polymers, the focus of this study was to broadly outline critical changes to the solid state structure and connect them to the mechanical properties of polyethylene with extent of rolling. Another aim in this work was to trace the initial spherulitic structure to the deformation morphologies observed by microscopy to refine the mechanistic picture of deformation on the microscale, as much of the prior work had focused on alteration of the nanostructure. Polyethylene has been selected for this study because, aside from its simple molecular architecture, HDPE cold rolled at room temperature is deformed between the beta relaxation or T_g at around −40 °C, and the crystalline melting temperature. Hence, the interlamellar and interspherulitic amorphous regions are expected to have sufficient mobility to deform under small strains where the crystalline regions would begin to deform plastically at larger strains. An improved mechanistic understanding of roll milling was sought out as a first step to optimizing the engineering design of such a process.

2. Experimental

2.1. Materials

Commercially compression molded 6.35 mm thick HDPE sheets were obtained from King Plastics Corporation (North Port, FL). According to the supplier, the sheets contained no additives. The molecular weight distribution of the material ($M_w/M_n = 9.55$) was characterized by GPC (Jordi Labs, Mansfield, MA), and it was determined that the M_w = 169,000 and M_z = 1,030,000. Sheets of 127 mm × 127 mm were cut by band saw to be cross-rolled.

2.2. Cross-rolling process

A two-high Fenn Rolling Mill with roll diameters of 26.7 cm and a roll speed of 6.1 s/revolution was used to cross-roll the material. The roll gap was set to reduce the thickness by 0.635 mm (or approximately 10% of the initial thickness) on every pass up to 10, and was reduced to accommodate the machine limits from 10 to 12 passes. The work piece was rotated 90° alternately clockwise and counterclockwise each pass, and two passes comprised a cross-pass (i.e. 1 × 1 for 2 passes, 2 × 2 for 4 passes, etc.). Cross-rolling took place at room temperature with unheated rollers. The sheet temperature was allowed to freely rise on each pass, and surface temperature was measured by IR thermometer. Shortly after every cross-pass, photos were taken of the sheets to measure width and length by digital image correlation using ImageJ software. Six sheets were rolled so that samples could be obtained at every cross pass from 1 × 1 through 6 × 6.

2.3. Light transmission

Light transmission was measured in the materials at larger extents of cross-rolling (i.e. 4 × 4, 5 × 5, and 6 × 6) using a PerkinElmer Lambda 1050 UV–Vis–NIR Spectrophotometer. The samples were coated with a thin layer of mineral oil to eliminate surface roughness.

2.4. Density measurement

Density was measured using a density gradient column utilizing a binary water-isopropanol system. The liquids were added to the column using the continuous fill method as per ASTM D1505. Samples were cut from approximately the same relative position in each cross-rolled sheet and from the core of the ¼" raw HDPE sheet material as a control.

2.5. Thermal analysis

Thermal analysis was performed by cutting 5–10 mg samples from approximately the same relative position of the cross-rolled sheets using a TA Instruments Q2000 Differential Scanning Calorimeter (DSC) utilizing a scan rate of 10 °C/min. Samples were cut from approximately the same relative position in each cross-rolled sheet and from the core of the ¼" raw HDPE sheet material as a control.

2.6. Oxygen permeability analysis

The oxygen barrier properties were measured for a 1/16" commercially compression molded sheet made from the same material and for the 6 × 6 cross-rolled material. Oxygen flux was measured using a MOCON OXTRAN® 2/20 at room temperature, 0% relative humidity, and 1 atm pressure.

2.7. Wide-angle X-ray scattering

2D wide-angle x-ray scattering (WAXS) patterns were obtained from the unrolled material as well as the material rolled to every cross-pass between 1 × 1 and 6 × 6 using a Xenocs Xeuss 3.0 Small-Angle Scattering/Wide-Angle Scattering (SAXS/WAXS) beamline. A Cu Kα radiation source (λ = 1.5406 Å) was utilized. Images were obtained with the x-ray beam oriented parallel and perpendicular to the plane of rolling. The 3 × 3 and 6 × 6 materials are depicted in Fig. 5a–d.

2.8. Small-angle X-ray scattering

2D small-angle x-ray scattering (SAXS) patterns were obtained from the unrolled material as well as the material rolled to every cross-pass between 1 × 1 and 6 × 6 using a Xenocs Xeuss 3.0 Small-Angle Scattering/Wide-Angle Scattering (SAXS/WAXS) beamline. A Cu Kα radiation source (λ = 1.5406 Å) was utilized. The 1 × 1, 3 × 3, 4 × 4, and 6 × 6 images with the x-ray beam oriented parallel to the plane of rolling are depicted in Fig. 6a–d and the 1 × 1, 4 × 4, and 6 × 6 images with the x-ray beam oriented perpendicular to the plane of rolling are depicted in Fig. 7a–c.

2.9. Mechanical properties

Tensile bars were cut from each material using an ASTM D1708 steel rule cutter die and drawn in tension to failure at room temperature using an MTS Insight® Electromechanical Testing System and at cryogenic temperatures using an Instron 5965 Universal Testing System at a strain rate of 100%/min. All tensile bars were cut along the length direction corresponding to the first roll pass direction. The environmental chamber of the Instron test system was cooled under conditions of forced air circulation to −40 °C using dry ice, and the sample was allowed to soak for 15 min prior to testing to allow the bulk temperature to equilibrate to that of the environmental chamber. Elastic recoveries were measured using digital image correlation from photos taken of the failed samples.

2.10. Dynamic Mechanical Analysis

Samples were prepared for dynamic mechanical analysis using a 10 mm wide steel rule rectangular cutter die. All specimens were cut along the length direction corresponding to the first roll pass direction. A single frequency temperature sweep was performed using a TA Instruments Q800 Dynamic Mechanical Analysis (DMA) Instrument, utilizing a dual cantilever sample clamp geometry. A temperature scan rate of 3 °C/min and a frequency of 1 Hz was used.

2.11. Scanning electron microscopy

A JEOL 6010LA Scanning Electron Microscope (SEM) was used to study the fracture surface morphology. A 6 nm conductive gold coating was deposited on the samples using a Quorum EMS150R ES Vacuum Sputter Coater. An accelerating voltage of 30 kV was used to capture SEM images.

3. Results and discussion

3.1. Observations from roll milling process

The thickness reduction as a function of roll passes is shown in Fig. 1, reflecting the extent of elastic thickness recovery measured shortly after each pass. Approximately 10–20% of the initial sheet thickness was recovered upon exiting the roll gap and the shape of the sheet thickness curve is bowed suggesting a peak in recovery around 6, or 3 × 3, rolling passes. Large elastic strain recovery of polyethylene upon exiting the deformation zone of a roll mill has been noted previously [22]. Table 1 shows the geometry of the HDPE sheets (width, length, and thickness) as a function of roll passes. The total sheet volume measured from these dimensions decreased up to 2 × 2 passes, followed by an increase up to 5 × 5 passes. The decreasing total volume at small strains suggests compaction, followed by expansion at large strains. The total thickness reduction measured after 12 passes was slightly above 80% of the initial sheet thickness, and decreased in a relatively continuous manner with roll gap reduction. Sheet lengths and widths, on the other hand, increased to a greater extent with increasing roll passes. Furthermore, the length and width did not increase evenly despite the equal reductions in the roll gap for every cross-pass, which would ideally impart balanced biaxial orientation to the sheet. The width of the sheets up to 6 × 6 passes (i.e. the rolling direction during even numbered passes) was consistently greater than the length attained on the pass preceding it. This is especially true of larger extents of rolling, as the degree to which the width increased relative to the length increased with consecutive rolling passes. This observation suggests that the viscous character of the material increased with rolling passes while the elastic character was subdued, as was later confirmed with dynamic mechanical analysis. Visually, buckling was prevalent in the material after 4 × 4 roll passes and became increasingly prominent up to 6 × 6 passes, suggesting that the material can increasingly recover larger strains along the width and length of the sheet with increasing roll passes (particularly after 3 × 3).

A large surface temperature rise was also observed upon rolling HDPE sheets. Fig. 2 shows a cross-plot of the surface temperature measured by an IR thermometer as well as the elastic thickness recovery

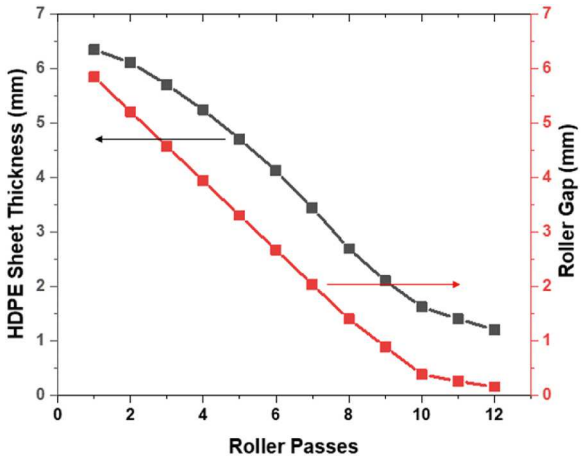

Fig. 1. Roller gap and sheet thickness measured after each pass through the rolling mill.

Table 1
Dimensional change in HDPE sheets with roll passes. Thickness is reduced by ~80% after 12 passes, width is increased by ~2.7X and length is increased by ~2.2X. The width direction is aligned to the second roll pass direction.

	Number of Passes	Thickness (mm)	% Thickness Reduction	Width & Length (mm x mm)	Volume Calculated (mm^3 $X10^4$)
HDPE sheet	**-**	**6.37**	**-**	**127 x 127**	**10.3**
1x1	**2**	**6.11**	**4.1**	**127 x 127**	**9.85**
2x2	**4**	**5.24**	**18**	**138 x 133**	**9.62**
3x3	**6**	**4.12**	**35**	**162 x 148**	**9.88**
4x4	**8**	**2.69**	**58**	**210 x 176**	**9.94**
5x5	**10**	**1.62**	**75**	**298 x 236**	**11.4**
6x6	**12**	**1.20**	**81**	**338 x 275**	**11.2**

measured shortly after each pass. The strain recoveries plotted in Fig. 2 are taken as the differences between the roll gap and measured thicknesses from Fig. 1. The surface temperature peaked at 5 × 5 passes before decreasing precipitously during the last two passes, likely due to the difference in roll gap reduction on the last two passes relative to those preceding them. Although non-adiabatic heat transfer mechanisms such as

conduction upon contacting the rollers should become more significant as the surface area to volume ratio increases, adiabatic temperature rise is known to result from the dissipation of mechanical work through slip mechanisms in crystalline polymers [23]. Bahadur et al. observed that the temperature rise in poly(oxymethylene) was greatest under cold rolling conditions, and rose to a lesser extent when the rolled material was preheated [24]. This result suggests that for crystalline polymers, the shear component of roll milling drives viscous dissipation via slip mechanisms, as the shear resistance would decrease with elevated temperature. Given the parabolic deformation profile for cold rolled materials [25], it is expected that the greatest dissipation would occur on the surface. Additionally, Salamatina et al. [26] had previously estimated the heat evolved from the deformation of the crystalline and amorphous regions of polyethylene by extrapolation of the heat evolved by degree of crystallinity at various strains. It was predicted by this method that almost no heat was evolved as a result of the deformation of the amorphous phase of polyethylene under conditions of pure compression. Therefore, the intense shear imparted on the rolled sheet and resulting activation of slip mechanisms and dissipation of mechanical work should be predominantly responsible for the temperature rise observed.

Between 3 × 3 and 4 × 4 passes, the material starts to buckle upon recovery and with each additional pass these buckles become more prominent. Additionally, the material becomes progressively more optically transparent from 4 × 4 to 6 × 6 passes. Qualitatively, these observations suggest that the lamellar crystals (which are sufficiently large to scatter light in isotropic, undeformed spherulites) have fragmented into smaller crystals between 3 × 3 and 4 × 4 rolling passes. Buckling on the other hand can likely be explained by the formation of a microfibrillar biaxial network upon lamellar fragmentation, which would be expected to drive an entropic recovery of the material after deformation. It is known that three distinct regimes exist in the deformation of polyethylene regardless of stress condition: the first is associated with amorphous deformation at small strains resulting in packing of amorphous chain segments with orientation (compaction), the second with the transfer of stresses across taut chains to crystals and crystal destruction by fragmentation (dilatation), and the third with the nucleation and growth of defects (cavitation) [27]. In Fig. 2, measured elastic recovery peaks at 3 × 3 passes, suggesting a cross-over in dominant mode of plastic deformation. At small strains, due to the compliance mismatch between the amorphous and crystalline phases, most strain will be accommodated in the amorphous regions by the processes of interlamellar separation and slip. However, at some critical amount of strain during compression and shear, the stress transferred to the crystalline phase will exceed its plastic yield strength, activating the chain and transverse slip processes. Furthermore, it has been suggested that chain slip, the dominant crystallographic deformation mechanism

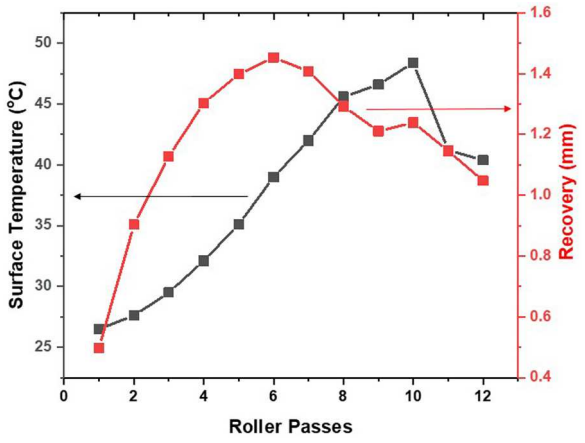

Fig. 2. Surface temperature measured by IR thermometer after each pass through the rolling mill plotted against elastic recovery of thickness after each pass. Adiabatic temperature rise results in a peak temperature just below 50 °C after 10 roll passes. Elastic recovery peaks at 6 passes, corresponding to an inflection point in the surface temperature rise.

in polyethylene regardless of stress condition, is largely reversible [20]. After localized slip processes occur [28], there is sufficient strain and mobility in the crystalline blocks to induce further irreversible amorphous deformation. It is therefore proposed that large scale fragmentation defines the boundary between two distinct regimes of deformation that lie on each side of the peak in measured recovery upon rolling, with small strains associated with limited irreversibility and a stronger restoring force. In the following section, the resulting cross-rolled sheets' physical and mechanical properties are characterized along with the structure on multiple length scales to further investigate the proposed deformation mechanism.

3.2. Physical properties

The increase in visible light transmission through the sheets during the later stages of cross rolling has been quantified using UV–Vis–NIR spectrophotometry. Fig. 3 shows the light transmission normalized for thickness in the visible range by calculating the attenuation coefficient for each wavelength and assuming the intensity of transmitted light decays exponentially with thickness. The greatest change in light transmission occurs between 4 × 4 and 5 × 5 passes for the entire spectrum of visible light. For all samples, a large step change is observed in the near UV light transmission (beginning at ~290 nm). However, a plateau in light transmission is also observed from about 375 to 500 nm in the 4 × 4 cross-rolled material as well. A larger step is present in the 4 × 4 light transmission at 290 nm. Because light scattering is driven by contrast in the refractive indices between the crystalline and amorphous phases, shorter wavelength light is expected to be more sensitive to smaller scattering features [29]. The amorphous structure is not expected to significantly contribute to scattering due to its small size relative to the wavelength of visible light [30]. It is therefore possible

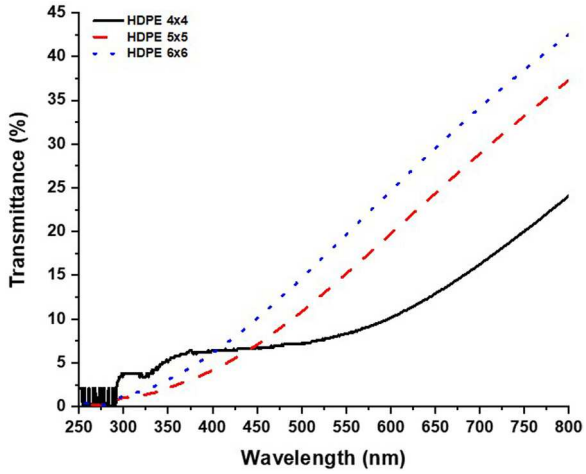

Fig. 3. Visible light transmission recorded using UV–Vis–NIR spectrophotometry. Transmission has been normalized to the thickness of the HDPE sheet rolled to 6 × 6 passes. The greatest change in light transmission occurs between 4 × 4 and 5 × 5 passes. Two step changes in the transmittance are measured after 4 × 4 passes (near 290 nm and 325 nm), and a single step change occurs after 5 × 5 and 6 × 6 passes (again at 290 nm).

that a finer distribution of crystal sizes is present after 5 × 5 passes due to lamellar thinning after fragmentation. It is also possible that some larger crystals in the 4 × 4 material responsible for the attenuation of larger wavelengths are destroyed or reduced in size after 5 × 5 passes. However, it is clear from this result that the increase in visible light transmission with cross-rolling is generally due to crystalline destruction, as undeformed lamellar crystals are of sufficient size to attenuate visible light [29].

To further investigate the change in structure upon rolling, densities and crystallinities were measured. Table 2 shows a decrease in density of about 0.012 g/cm^3 after 6 × 6 rolling passes. Table 2 also

shows the calculated crystallinity as a function of roll passes assuming a biphasic model for polyethylene, where the crystalline density is 1.000 g/cm^3 and the amorphous density is assumed to be 0.855 g/cm^2. Crystallinities as a function of roll passes were measured by DSC from the melting endotherms, assuming a heat of fusion of 290 J/g for single polyethylene crystals [31]. The decrease in crystallinity as measured by DSC is about 7% by weight as compared to about 8% by weight calculated from the two-phase model. The density reduction must be driven by some combination of crystalline destruction and void formation [32], the latter having little influence on the crystallinity measured by DSC. One possibility for the offset observed between the crystallinity calculated from the two-phase density model and by measurement from DSC is the assumption of an inappropriately small amorphous phase density. The crystallinity calculated from the ratio of WAXS peak intensity to that of the amorphous halo for the un-rolled material closely matched that measured by DSC at 66.7%, suggesting that the amorphous phase density selected for the two-phase model may have been too low for the isotropic material (0.885 g/cm^3 is necessary to match the calculated crystallinity to that measured by DSC and WAXS). Furthermore, the calculated density required to match the DSC measured crystallinity at every roll pass tracks quite well with the sheet volume change reported in Table 1. Amorphous compaction during the initial stages of rolling worsen the accuracy of the two-phase model, but improve its accuracy during the second dilatational phase of roll deformation. After 4 × 4 roll passes, the calculated amorphous phase density to match the DSC measured crystallinity steadily increases with additional cross-rolling up to 6 × 6 passes, suggesting further compaction of the amorphous phase at large extents of rolling. Furthermore, the close agreement between DSC measured crystallinity reduction vs. crystallinity reduction calculated using the biphasic model suggests that the loss of density is primarily driven by the generation of amorphous material due to the destruction of crystals rather than by the formation of voids.

Peak melting temperatures are also reported in Table 2, as calculated from the DSC thermograms plotted in Fig. 4 which have been offset on the ordinate for the sake of convenient comparison. The peak melting temperature remains steady in the initial stages of rolling followed by a decrease. In the terminal stages of rolling in this experiment, the peak melting temperature again increases. The steady decrease in peak melting temperature from approximately 1 × 1 to 4 × 4 passes suggests that lamellar thinning is a prominent feature of the initial deformation regime in cold rolling. This seems to change abruptly following 4 × 4 passes when the peak melting temperature begins to increase from 5 × 5 to 6 × 6 passes. Lamellar thinning during the initial stages of deformation are likely a consequence of lamellar tilt and thinning that precedes the large scale discontinuous fragmentation process occurring at larger strains [28]. It is possible that following fragmentation, annealing is responsible for the increase in peak melting temperature observed. As will be later seen, the surface temperature has reached a point very close to the peak α-relaxation temperature by 5 × 5 passes.

These observations again suggest a shift in deformation regime from one associated with compaction as well as lamellar rotation and tilt to

Table 2
Density and crystallinity reduction with cross-rolling passes. The density is reduced in a sigmoidal manner. Crystallinity is calculated from density using the biphasic model, but overestimates the crystallinity measured by DSC. The difference is likely due to an underestimate of the amorphous phase density in the biphasic model assumption.

Rolling Passes	Density (g/cm^3 ± 0.0003)[a]	Crystallinity from Density (% ± 0.2)[b]	DSC Crystallinity (% ± 1)[c]	Tm (°C ±0.5)	P(O_2) (Barrer Units ± 0.07)
Control	0.959	74.8	67	134	1.02
1x1	0.959	74.8	66	134	–
2x2	0.958	74.1	67	134	–
3x3	0.955	72.2	65	133	–
4x4	0.951	69.6	65	132	–
5x5	0.948	67.7	62	132	–
6x6	0.947	67.0	60	133	0.452

[a] Determined by ASTM D1505 density gradient column method.
[b] Weight basis, calculated from densities where $\rho_{amorphous}$ = 0.855 g/cc, $\rho_{crystalline}$ = 1.000 g/cc.
[c] Weight basis, measurement from DSC melting endotherm.

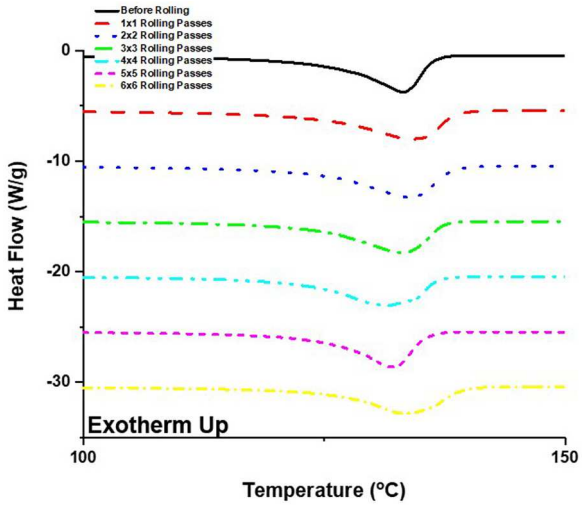

Fig. 4. DSC thermograms of HDPE after varying numbers of rolling passes. The melting endotherm broadens after 1 × 1 passes, steadily decreases from 2 × 2 to 4 × 4 passes, and then increases from 5 × 5 to 6 × 6 passes.

one dominated by fragmentation and dilatation.

Permeability experiments showed a reduction in the oxygen permeability of the 6 × 6 cross-rolled material by more than a factor of two when compared to the same melt extruded HDPE. This decrease in small molecule permeability is probably driven by the increased small molecule diffusion path length following fragmentation. A familiar example would be composites making use of inorganic fillers to improve barrier properties in an analogous way [33]. However, it is also a possibility that amorphous compaction plays a role as well. As suggested previously in the comparison between the crystallinities calculated from densities using a two-phase model vs. those measured by crystallinity, amorphous phase compaction occurs not only in the initial compaction regime of deformation at small thickness reductions, but also from 4 × 4 to 6 × 6 passes. Due to the diffusion of small molecules through only the amorphous phase, the amorphous structure is expected to have some bearing on overall permeability in addition to the change in diffusion path length resulting from crystalline morphology. Vapor permeability measurements normalized for the amorphous fraction (as measured by DSC) in metallocene LLDPE by Srinivas and Brant [34] have been used to show that amorphous densification is possible upon orientation. Due to the prohibitively large thickness of sheets cross-rolled less than 6 × 6 passes, permeability analysis could not be performed on these samples and the control was taken as a thinner extruded section of the same resin. However, it would be interesting to determine whether or not small molecule diffusion is affected in the initial stages of rolling in the future.

A final point is that the improvement in barrier properties with rolling suggests that void formation may be suppressed during the dilatational deformation regime. Presumably, any voids generated during cross-rolling would have to be nano-sized, and hence too small to scatter visible light given that the material does not whiten upon deformation. The same conclusion can be drawn from the comparison between DSC measured and calculated crystallinities from the two-phase model given a similar reduction in crystallinity calculated by each method. Therefore, the free volume of the amorphous phase may change with roll deformation but it is unlikely that voids contribute significantly to the rolled material's permeability behavior.

3.3. 2D wide-angle X-ray scattering

2D WAXS patterns were obtained to study the effect of cross-rolling on the crystal orientation. In Fig. 5a–d, 2D WAXS patterns are shown of the HDPE sheets after 3 × 3 and 6 × 6 rolling passes for the x-ray beam directed in the plane of rolling (5a,b) and perpendicular to the plane of rolling (5c,d). When the beam is directed parallel to the plane of rolling, sharp isotropic Debye rings corresponding to the (110) and (200) orthorhombic crystal planes are observed. A weaker diffraction ring corresponding to the (001) monoclinic crystal plane is also present. The presence of a monoclinic phase had been found previously in compressively deformed polyethylene, and is attributed to a phase transformation from the orthorhombic to the monoclinic form due to tensile stresses perpendicular to the chain direction induced upon rapid unloading. [17,21,35]. After 3 × 3 rolling passes, weak (110) four-point intensity maxima appear about 30° from the equator in addition to broad (110) and (200) two-arc patterns. After 6 × 6 rolling passes, the (110) reflection sharpens and a four-point pattern becomes well defined in the (200) ring as well. For each of these, the intensity maxima shift to about 40° to either side of the equator. Sharper (110), (200), and (001) two-arc patterns are now visible after 6 × 6 passes. In both the orthorhombic and monoclinic crystal planes, the two-arc pattern suggests slight c-axis orientation towards the plane of rolling. The four off-axis maxima have been associated with tilted lamellae [36], and the movement of these maxima towards the meridian from 3 × 3 to 6 × 6 passes suggest that tilting progressively increases towards the roll direction with thickness reduction.

In comparison, when the beam is oriented perpendicular to the plane of rolling (Fig. 5c and d), isotropic diffraction rings are observed for the (200) and (110) orthorhombic as well as the (001) monoclinic crystal planes after both 3 × 3 as well as 6 × 6 rolling passes. This indicates that the rolled sheets exhibit planar isotropy, or uniplanar orientation as a result of cross-rolling which is a common feature of balanced biaxially cold rolled semicrystalline polymers [25].

3.4. 2D small-angle X-ray scattering

2D SAXS patterns were obtained to understand the lamellar orientation with cross-rolling. In Fig. 6a–d, patterns are depicted with the x-ray beam taken parallel to the plane of rolling. Fig. 6a reveals a circular scattering pattern, indicating that there is no preferred lamellar orientation at 1 × 1 passes. Fig. 6b on the other hand reveals an elliptical pattern with the short axis on the equator. It is suggested that lamellar separation of polar lamellae combined with lamellar slip of equatorial crystals led to the distortion of the scattering pattern due to the difference in long period spacing in the two directions [5]. The emergence of a four-point pattern also suggests that lamellae had been tilted and deformed by kinking to produce a chevron type texture. Such an explanation had been given to the four-point SAXS pattern previously for polyethylene rolled unidirectionally [19]. By 4 × 4 passes, the four-point pattern begins to weaken and develop into a two-point meridional pattern as seen in Fig. 6c. The development of a two-point pattern is interpreted alongside the 2D WAXS patterns presented in the previous section to indicate that following fragmentation, lamellae are sufficiently mobile to be oriented in the direction of rolling. It seems that further orientation occurs in the direction of rolling from 4 × 4 to 6 × 6 passes, given that the elliptical pattern further elongates in the meridional direction as seen in Fig. 6d.

Fig. 7 depicts 2D SAXS patterns taken with the x-ray beam direction perpendicular to the direction of rolling. In Fig. 7a, again a circular scattering pattern is seen after 1 × 1 passes indicating no preferred lamellar orientation in the plane of rolling. The scattering intensity is reduced and a new two-point scattering feature emerges after 4 × 4 passes as depicted in Fig. 7b. Previously, the emergence of this new scattering feature was attributed to fibrillation during rolling [37]. It is similarly proposed that freshly fragmented lamellae are oriented in the previous roll direction that have not yet been randomized in the plane of rolling, and that the scattering intensity is diminished due to the process of fragmentation and subsequent dispersion or reorientation across the plane of rolling. By 6 × 6 passes, as depicted in Fig. 7c, the scattering intensity is weakened even further and it is at this point that fragmentation has been maximized.

The lamellar long period spacing in the terminal roll direction for each cross-pass was calculated from the first order intensity maxima. It was found that before rolling through 3 × 3 passes, the long period spacing in this direction was about 33 nm. After 4 × 4 passes, the long period spacing abruptly rose to 36 nm and then settled at 30 nm after 10 and 12 passes. It is possible that lamellar thinning due to tilt is responsible for the abrupt increase in long period. After fragmentation occurs, a new long period is established which is smaller than that of the un-fragmented lamellar crystals.

3.5. Mechanical properties

The engineering stress strain curves for HDPE sheets at various thickness reductions obtained at both room temperature (25 °C) as well as under cryogenic conditions (−40 °C) are shown in Fig. 8a and Fig. 8b.

The tensile properties are defined graphically in Fig. 9 and reported both up to yield and after yield to fracture in Table 3a and Table 3b respectively. Under room temperature conditions, abrupt yield behavior is observed before rolling resulting in localized strain and whitening. The neck formed upon yielding propagated along the gauge length, then the material underwent work hardening until failure. This behavior persisted with increasing thickness reduction until 4 × 4 passes, when a

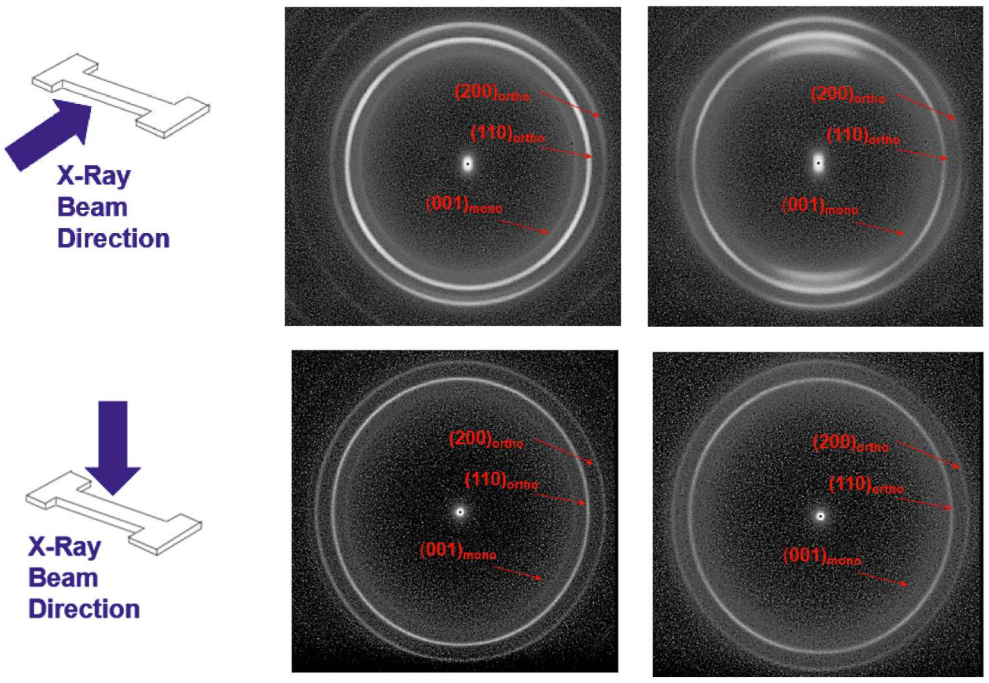

Fig. 5. Edge-on 2D WAXS patterns are depicted for a) HDPE rolled to 3 × 3 passes (top left) and b) 6 × 6 passes (top right). Flat-on 2D WAXS patterns are depicted for c) HDPE rolled to 3 × 3 passes (bottom left) and d) 6 × 6 passes (bottom right). Band splitting can be seen in 5b due to slight orientation.

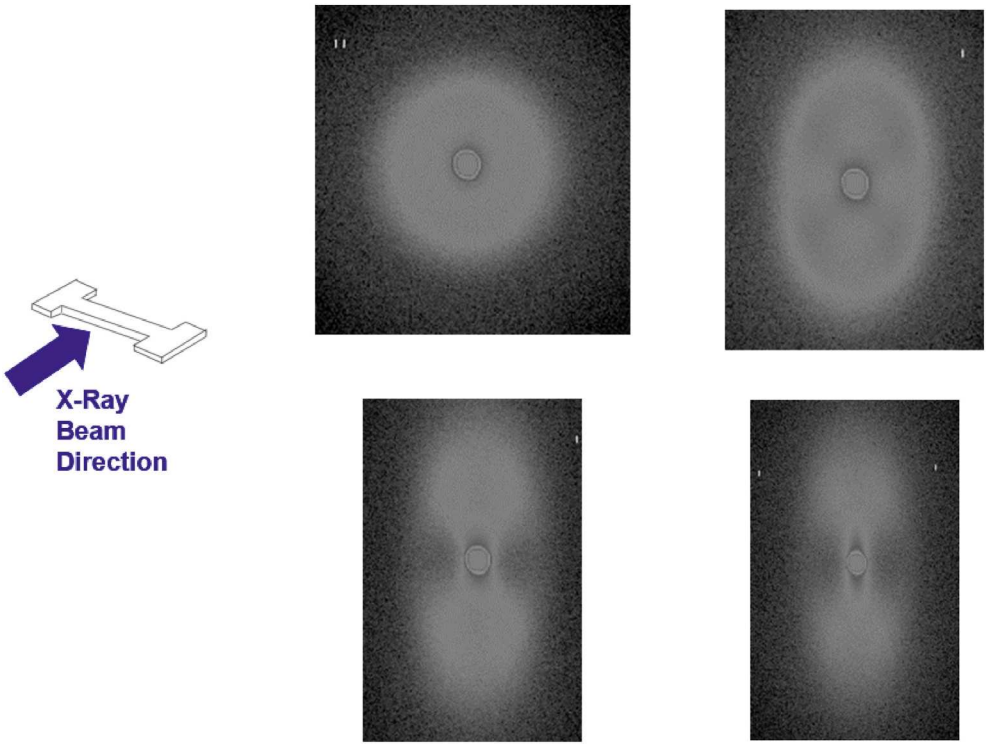

Fig. 6. Edge-on 2D SAXS patterns depicted for a) HDPE rolled to 1 × 1 passes (top left), b) 3 × 3 passes (top right), c) 4 × 4 passes (bottom left), and d) 6 × 6 passes (bottom right). A circular pattern progressively elongates into an ellipse with an equatorial short axis. A four-point pattern also emerges early in the deformation, but gradually gives way to meridional intensity maxima, suggesting that tilt and lamellar kinking precede fragmentation and lamellar orientation in the roll direction.

gradual yield process was observed which did not involve strain localization or whitening, instead revealing homogeneous deformation in the cross-section of the gauge length. A similar non-whitening, gradual yield process is known to take place in plastomeric or so-call "Type II" polyethylene [31]. The same yield behavior is observed at −40 °C after cross-rolling, increasing the ductility of the material greatly relative to the unrolled HDPE sheet. The shift from an abrupt to a diffuse yield mechanism as well as a large increase in the elongation to failure has been observed under cryogenic conditions in cross-rolled polypropylene [13]. Table 3b shows a remarkable increase in the work hardening

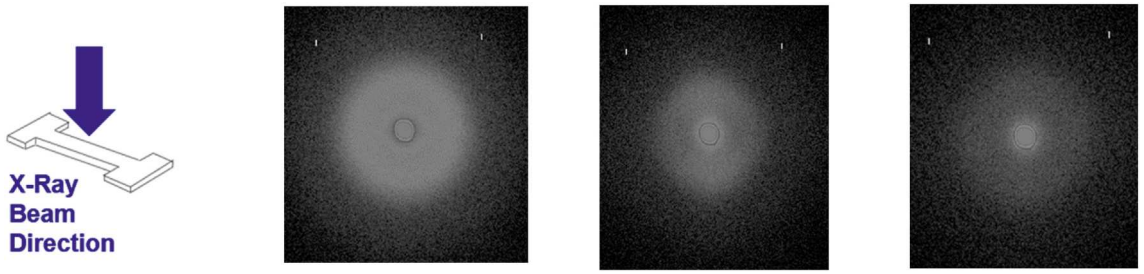

Figs. 7. 2D SAXS patterns taken with the x-ray beam perpendicular to the plane of rolling after a) 1 × 1 roll passes (left), b) 4 × 4 roll passes (center), and c) 6 × 6 roll passes (right). The scattering intensity progressively diminishes with rolling, suggesting reorientation of lamellae. The emergence of a short-lived two-point pattern after 4 × 4 passes suggests large scale fragmentation at this point.

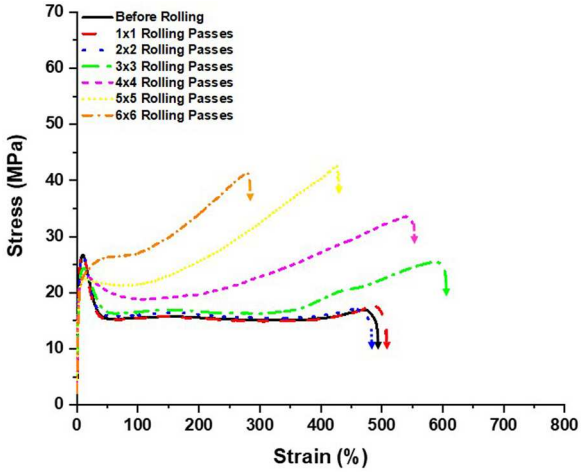

Fig. 8a. Engineering stress-strain curves showing the effect of cross-rolling on the tensile behavior at 25 °C and 100%/min strain rate. Before rolling, abrupt yield behavior is observed. After 4 × 4 rolling passes, yielding becomes progressively more diffuse. Work hardening and tensile strength are increased with increasing rolling passes up to 6 × 6.

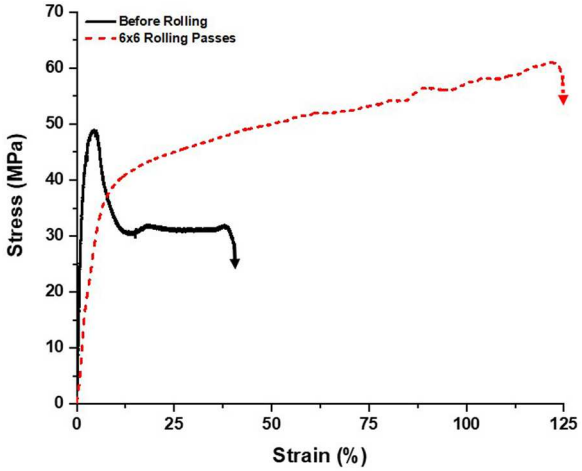

Fig. 8b. Engineering stress-strain curves showing the effect of cross-rolling on the tensile behavior at −40 °C and 100%/min strain rate. Before rolling, a neck forms but does not propagate along the gauge length before brittle fracture occurs, resulting in a low elongation to failure. After 6 × 6 rolling passes, diffuse yield behavior and work hardening are observed.

modulus and also fracture stress, particularly after 3 × 3 passes at room temperature. The work hardening modulus of semicrystalline polymers drawn under conditions of plane-strain using a channel die had been

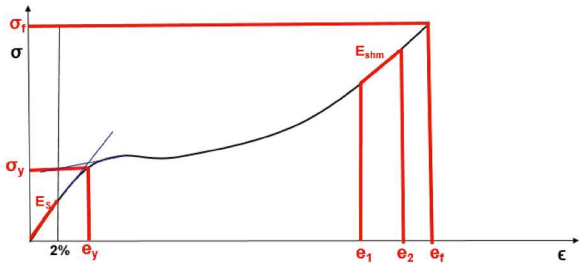

Fig. 9. Key mechanical properties are calculated as follows: 1) 2% secant Young's modulus (E_s), 2) Yield strain (e_s) and corresponding yield stress (σ_s) at the intersection of tangent lines, 3) Strain hardening modulus between two points in the linear work hardening region, and 4) Failure stress (σ_f) and corresponding failure strain (e_f) at the maximum before failure.

Table 3 a)
Tabulated tensile properties both under room temperature (25 °C) and cryogenic (−40 °C) conditions up until yield. The yield mechanism changes from abrupt to diffuse, leading to the disappearance of a neck at 4 × 4 roll passes. The modulus and yield stress decrease slightly with progressive rolling passes.

Rolling Passes	Temperature (°C)	Necking	E_S (GPa) ±0.08 GPa	σ_y (MPa) ±1 MPa
Control	**25**	**Yes**	**0.76**	**27**
1x1	**25**	**Yes**	**0.78**	**27**
2x2	**25**	**Yes**	**0.84**	**26**
3x3	**25**	**Yes**	**0.80**	**24**
4x4	**25**	**No**	**0.77**	**23**
5x5	**25**	**No**	**0.73**	**22**
6x6	**25**	**No**	**0.74**	**21**
Control	**−40**	**Yes**	**2.1**	**49**
6x6	**−40**	**No**	**0.93**	**36**

studied, and it was concluded that the increase in work hardening is associated with the preservation of entanglements under these conditions. For crystalline polymers containing crystals with lower plastic resistance, the material will yield by the deformation of crystals rather than by amorphous disentanglement [7]. In contrast, the deformation of isotropic spherulites in uniaxial tension results in cavitation due to the presence of stress risers associated with the higher plastic resistance of polar vs. equatorial lamellae, and subsequent disentanglement resulting in far lower work hardening stiffness [5]. Such intense localization of strain increases softening at the yield point and reduces work hardening (c.f. cross-rolled polyethylene which exhibits diffuse yield behavior and increased strain hardening due to its enhanced capacity to delocalize strain). It has been demonstrated that the ratio between post-yield softening and work hardening govern a polymeric material's intrinsic stress response (i.e. brittle or tough) and its ability to accommodate large or small strains after yielding [38]. In the case of crystalline polymers, it is likely that at room temperature the unravelling of

Table 3 b)
Tabulated tensile properties both under room temperature (25 °C) and cryogenic (−40 °C) conditions from yield to fracture. The work hardening modulus and fracture stress notably increase with progressive rolling passes. The elongation to failure peaks at 3 × 3 passes and is reduced with additional rolling passes.

Rolling Passes	Temperature (°C)	E_{shm} (MPa) ±1.5 MPa	σ_f (MPa) ± 4 MPa	e_f (%) ±175%	DR (volumetric) at fracture±0.3 MPa	Elastic Recovery (%) ±7%
Control	**25**	**3.0**	**17**	**500**	**6.4**	**7.3**
1x1	**25**	**3.6**	**17**	**430**	**6.3**	**10**
2x2	**25**	**3.3**	**18**	**500**	**6.4**	**7**
3x3	**25**	**5.0**	**28**	**650**	**7.9**	**10**
4x4	**25**	**5.3**	**33**	**540**	**7.2**	**18**
5x5	**25**	**8.6**	**43**	**430**	**6.2**	**24**
6x6	**25**	**11**	**43**	**300**	**4.7**	**18**
Control	**−40**	**0**	**32**	**38**	**3.4**	**2.4**
6x6	**−40**	**19**	**61**	**120**	**2.3**	**23**

spherulitic crystals during the formation of a microfibrillar texture upon rolling limits the extension to failure. However, at cryogenic temperatures (near the glass transition temperature), it is possible that the intrinsic toughening due to strain delocalization is the dominant factor in the material's elongation to failure.

Remarkably, the elastic recovery upon failure increases dramatically with cross-rolling under cryogenic conditions. Recalling the large strain recoveries observed upon roll milling, each process involves deformation at a rapid rate relative to the chain relaxation time scale. An increase in the strain recovery with cross-rolling is also observed under room temperature conditions, but not to the same extent (increase by a factor of two vs. a factor of ten), likely due to the higher draw ratio attained at the higher draw temperature. Stress must be transferred between a combination of entanglements relegated to the amorphous region and physical cross-links (i.e. lamellar bundles), and the entropic deformation of the amorphous material should primarily drive the recovery. Hence, the drastic increase in elastic recovery at both temperatures supports the biaxial crystalline network structural model. Furthermore, the persistence of strong elastic recovery at temperatures near the beta relaxation (or glass transition temperature) support the continuum deformation model associated with strain delocalization, as strong strain localization results in disentanglement in deformation zones taking the form of craze fibrils [39].

The 2% secant Young's modulus does not appreciably change with cross-rolling, and perhaps decreases slightly. Like the work hardening modulus, the Young's modulus is also dependent upon the molecular weight of chain segments between physical cross-links and entanglements [40]. It is expected that in the process of cross-rolling, the average molecular weight between lamellar bundles in the network are increased due to conversion of the crystalline chain segments into amorphous segments as well as some disentanglement associated with deformation of the amorphous phase, resulting in a decrease in the modulus. Furthermore, the stress response during crystal slip should be influenced by lamellar thickness which may be another reason why modulus decreases after rolling [5]. The yield stress also decreases with cross-rolling, likely due to the decreased plastic resistance of the crystals following fragmentation of the lamellae [7].

The draw ratio is maximized at 3 × 3 roll passes, and then decreases with subsequent rolling up to 6 × 6 passes under room temperature conditions. As the crystallinity decreases upon further rolling between 3 × 3 and 4 × 4 passes, dramatically less cold drawing is observed suggesting that the crystalline phase of the material is able to accommodate less deformation in tension before disentanglement must occur and the material fails. Snyder et al. [13] concluded that for cross-rolled polypropylene under cryogenic conditions, the elongation to failure is increased due to the presence of a circular damage zone capable of accommodating higher loads than the narrow damage zone observed in the absence of cross-rolling. This study elucidates the importance of higher-order structure on the mechanical properties, which will be discussed in more detail in the section reporting analysis of the fracture surface.

3.6. Dynamic mechanical analysis

The loss tangent and loss modulus measured by constant frequency temperature sweep dynamic mechanical analysis is shown in Fig. 10a and Fig. 10b respectively. A few important structural observations can be inferred from these plots. The first relates to the decrease in the loss tangent with increasing temperature following the alpha peak temperature beginning at 4 × 4 passes. Furthermore, a broad beta relaxation peak temperature can be seen in Fig. 8b in the unrolled material at about −40 °C. After 3 × 3 rolling passes, this peak shifts to a higher temperature (about −10 °C). However, after 4 × 4 rolling passes, instead of a beta relaxation peak, a steady decrease in the loss modulus with temperature is seen. As previously mentioned, perfectly balanced biaxial orientation was not attained likely due to this softening effect. These observations collectively suggest that the evolution of a microfibrillar texture due to lamellar fragmentation indeed occurs between 3 × 3 and 4 × 4 passes. Under the deformation of spherulitic lamellar crystals in compression and shear, one would expect compaction of the interlamellar amorphous material in the initial stages of rolling, which would tauten interlamellar tie chains and increase the activation energy for the beta process(i.e. raise the peak temperature). At sufficiently high strains, the chains would remain taut but be constrained in a biaxial microfibrillar network, unable to relax; hence the disappearance of the beta relaxation peak. Furthermore, the alpha relaxation peak temperature in Fig. 8a remains at about 75 °C up until 4 × 4 rolling passes, and is then lowered with additional cross-rolling. Because the alpha process peak temperature is related to both the lamellar thickness as well as surface disorder [31], this observation suggests that the increase in surface disorder may be responsible for the decrease in the peak alpha relaxation temperature after 4 × 4 passes, as annealing and lamellar

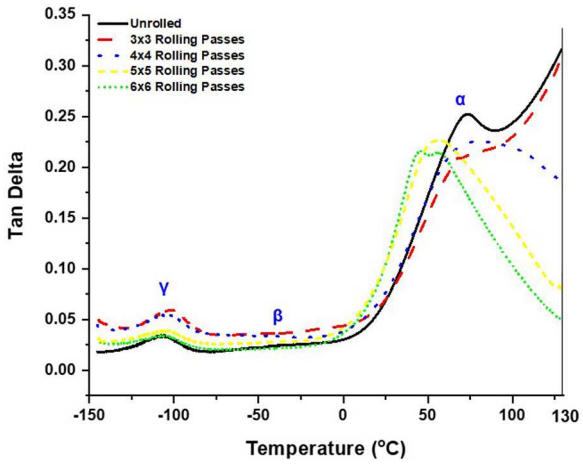

Fig. 10a. Constant frequency temperature sweep dynamic mechanical analysis. Diminishing loss tangent with temperature following the alpha relaxation peak after 4 × 4 passes is depicted.

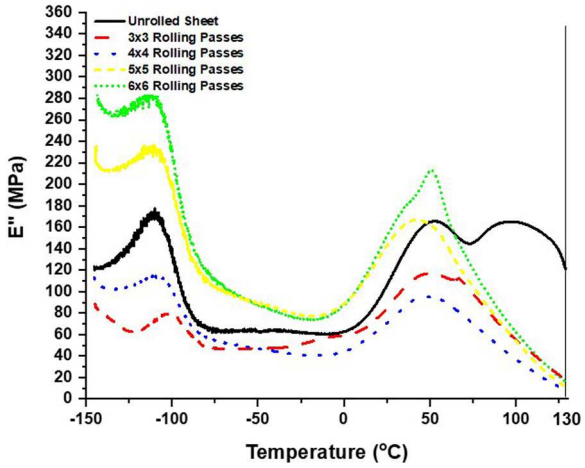

Fig. 10b. Constant frequency temperature sweep dynamic mechanical analysis. A plot of loss modulus vs. temperatures shows the elimination of the beta relaxation peak after 4 × 4 passes.

thickening seem evident from the thermal results. This process requires that the amorphous chains tying together the fragmented lamellar crystals must be taut enough to transfer sufficient stresses to result in plastic deformation of the crystalline region. Hence, crystal deformation rather than amorphous characterizes the dilatational regime of plastic deformation.

3.7. Analysis of the fracture surface

The fracture surface of a tensile bar cut from the HDPE sheet rolled to 6 × 6 passes and fractured in tension at −40 °C was studied in detail. In Fig. 11, an SEM micrograph of the end of one fracture surface is shown. It is clear that three visually distinct zones are present on the fracture surface. Zone I as will be described in detail is the damage zone, and Zones II & III are each surfaces generated by the propagation of the crack during failure, albeit at different rates. As such, the direction of crack propagation progresses from right to left, and Zone III is the terminal zone preceding failure. Fig. 12a shows a magnification of Zone I, revealing delaminated microlayers and some interconnecting submicron fibrils. These fibrils are in the range of 200–500 nm, measured using digital image correlation software. A magnified image of the interface between Zones I and II is shown in Fig. 12b, again revealing the presence of delaminated microlayers but also the presence of an increased density of interconnecting submicron fibrils. About forty sample points were processed using digital image correlation software (ImageJ), and it was found that the mean size of these fibrils were 200 μm with a standard deviation of 50 μm. Remarkably in Zone II, microlayers are no longer present and instead a dense network of submicron fibrils with a narrow size distribution are present as shown in Fig. 12c. After a similar analysis using digital image correlation, it was determined that a mean fibril size of 270 μm with a standard deviation of 60 μm are present in the micrograph. It is likely that the crack propagation in this initial zone of failure is slow enough to delaminate the material along weaker interfaces present, resulting in a dense, interconnected fibrous network. It is also interesting to note that the dominant orientation of these submicron fibers appears to be in the lateral direction, again suggesting their precursors were the layers visible in the transition zone between I and II. It is expected that as the surface area of the un-fractured material

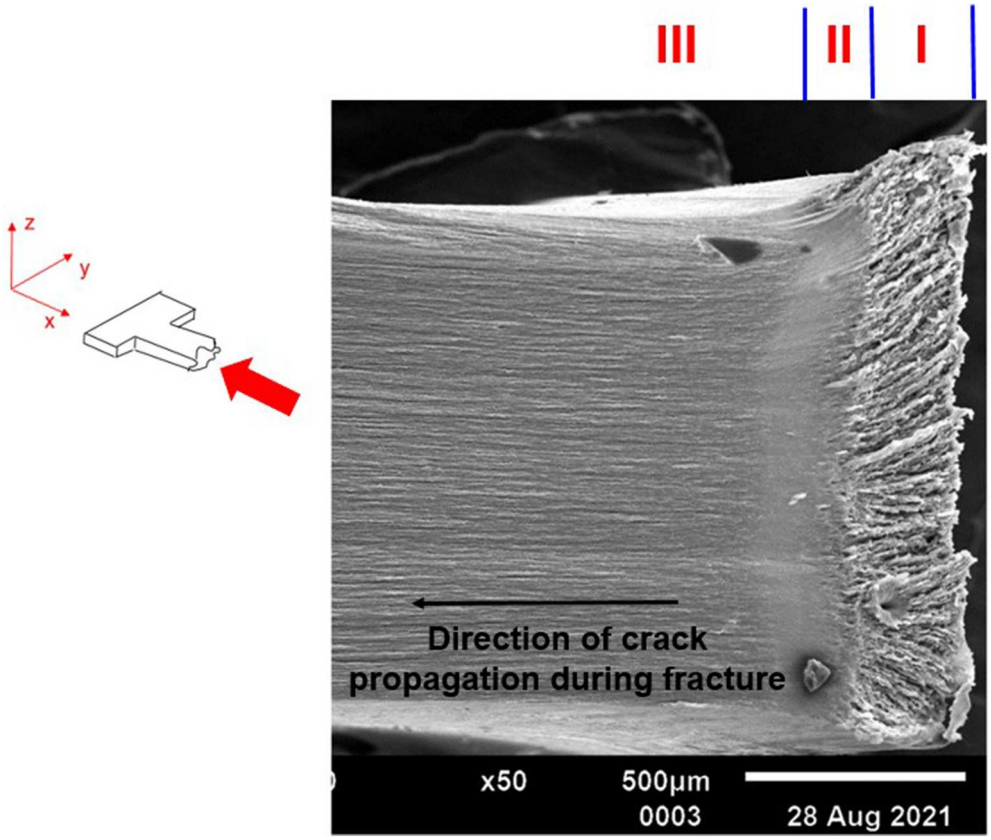

Fig. 11. SEM image of surface of HDPE rolled 6 × 6 passes fractured in tension at −40 C. The fracture surface can be divided into 3 distinct regions: I) The damage zone formed prior to crack propagation, II) The region at the end of the damage zone corresponding to slow crack growth rate, and III) The terminal region of failure corresponding to rapid crack propagation.

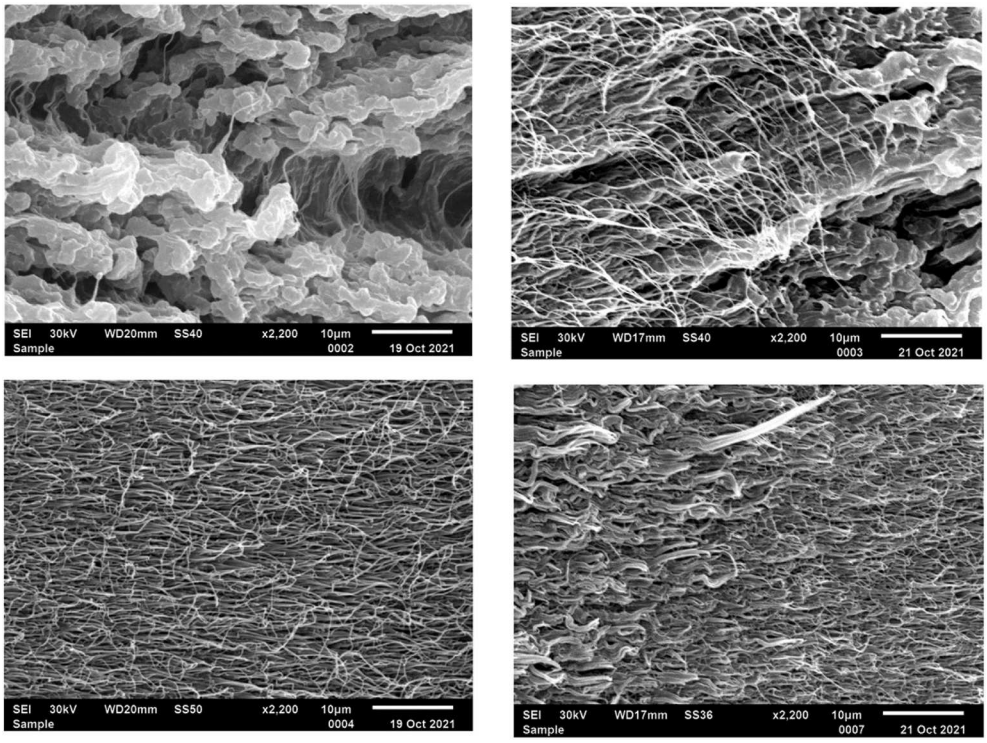

Fig. 12. Magnified SEM image of a) Zone I (the damage zone), showing delaminated layers and submicron interconnecting fibrils (top left), b) The interface between zones I & II (top right). Moving from zone I to zone II, the number of interconnecting fibrils between delaminated layers increases abruptly until only fibers are present. Torn layers are evident at the interface, suggesting that interconnecting fibrils originated from the layers. Fig. 12 c) depicts Zone II (region at the end of the damage zone), showing a network of interconnecting submicron fibrils (bottom left). Fig. 12 d) depicts the interface between zones II & III (bottom right). As with the interface between zones I & II, the interconnecting fibrils can be traced back to dilated and buckled microlayers. The rate dependence of morphology in each zone is made clear here; the crack propagation in the terminal zone is too rapid to pull the material into a fibrous network, and buckles upon recovery.

decreases and the true stress rises, the rate of crack propagation will increase. Hence, in the transition between Zones II and III, as shown in Fig. 12d, delaminated microlayers are again increasingly present past the transition, but with a buckled appearance.

Fig. 13a shows the bulk of Zone III where a rapid failure process is expected to have occurred. Again, evidence of recoil resulting from the rapid failure process is evident in the form of transverse buckling from the end view of the fracture surface. Because dilatational stresses and strains are present at the crack tip, a recoil response would be expected in the transverse direction as well as the machine direction when drawn in tension. A dense craze network has previously been identified in the damage zone of cross-rolled polypropylene [13]. Furthermore, a weaker thickness direction is expected given the orientation observed by WAXS in the rolling plane, indicating uniplanar molecular orientation. Hence, the presence of dilatational stresses and strains at the craze tips and crack tip in the damage zone and fracture surface respectively can explain delamination along the thickness direction. In the case of Zone III, the recoil along the transverse direction is presumably the result of a recovery process exclusively along the rolling plane and irreversible deformation caused by a volume generating (i.e. void forming) process near the fracture surface during damage zone formation and subsequent failure.

Fig. 13b, depicting Zone III at a higher magnification, reveals submicron layers on the size scale of 800 nm (with a standard deviation of 160 nm) within the large delaminated microlayers. It is possible that these features are the result of deformed spherulites, as suggested by Osawa et al. [14] in the case of compressively deformed iPP. Assuming that the layers were affinely deformed during the cross-rolling process, the approximate diameter of the spherulites would be expected to be about 4 μm, which is a reasonable assumption for polyethylene [5].

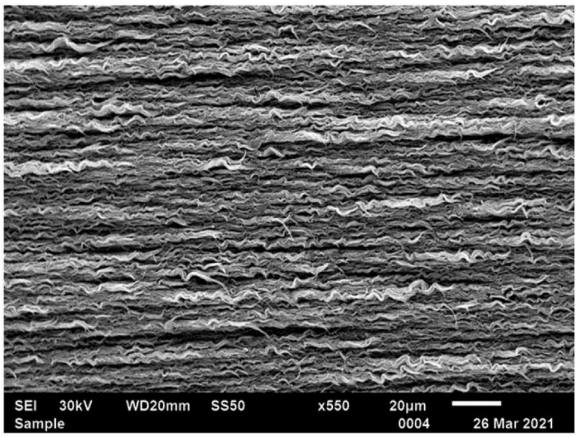

Fig. 13a). Magnified image of zone III, corresponding to rapid crack propagation just before failure. At increased magnification, it is evident that microlayers had separated during the fracture event as well as recoiled along the transverse direction.

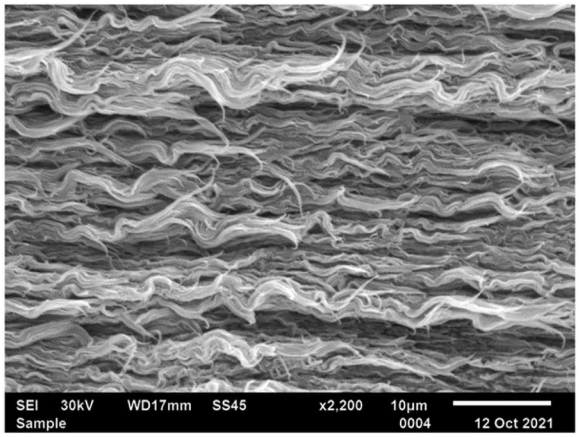

Fig. 13b). Further magnified image of zone III, showing delaminated submicron layers cooperatively buckled within the delaminated microlayers. The buckling phenomenon is a consequence of the strong elastic recovery resulting from the rapid failure and release of stress.

4. Conclusions

It can be concluded that cold-rolling polyethylene in a balanced biaxial manner occurs in two distinct regimes. The first is deformation by interlamellar separation and slip alongside lamellar tilt and crystal slip, ultimately resulting in compaction at small thickness reductions. The second is deformation primarily by the destruction of crystals in a dilatational process at larger strains. Despite the complex deformation mechanism of polyethylene during the cold rolling process, this work defines two distinct regimes resulting from the collective outcomes of these processes. At small deformations, this process tautens the interlamellar amorphous material as a consequence of interlamellar slip and separation resulting in a reduction in free volume in the region (i.e. amorphous compaction). Lamellae are also kinked and tilted in a continuous deformation process in the first regime. However, at some critical point, localized, catastrophic deformation of the crystalline lamellae occurs by fragmentation and a fibrillar structure is allowed to form. At this critical point, deformation hence proceeds in a fundamentally different way. This work also proposes that both regimes of deformation progress within the original spherulitic boundaries which affinely deform during the rolling process as evidenced by scanning electron microscopy. Such an admittedly simplified scheme may provide a framework for engineers to develop new designs and further optimize the cold rolling process for crystalline polymers.

CRediT authorship contribution statement

N. McMullen: Investigation, Writing – review & editing. **C. Zhang:** Investigation, Validation. **C. Cheng:** Formal analysis. **G.E. Wnek:** Project administration, Supervision. **A. Olah:** Validation, Visualization, Supervision. **E. Baer:** Conceptualization, Methodology, Supervision.

Declaration of competing interest

The authors declare the following financial interests/personal relationships which may be considered as potential competing interests: Eric Baer, Andrew Olah, Gary Wnek, Cong Zhang, and Nathan McMullen have patent pending to Case Western Reserve University.

Acknowledgements

The authors are grateful for the generous support from the US Army Research Lab (ARL) via Contract #W911NF2020155. The authors would also like to thank collaborators at DEVCOM Army Research Lab, Aberdeen Proving Ground, MD and would like to extend a special thanks to Dr. Dayne Plemmons of ARL for his ongoing support at Case Western Reserve University. The authors acknowledge access to the X-ray scattering facility at the Advanced Materials and Liquid Crystal Institute (AMLCI) at Kent State University, which was financially supported by the National Science Foundation (DMR-2017845), the State of Ohio (The Ohio Department of Higher Education Action Fund), and Kent State University.

References

[1] W.L. Roberts, Cold rolling of steel, Marcel Decker (1978) 16–26.
[2] W.A. Backofen, Deformation processing, Metall. Mater. Trans. B 4 (12) (1973) 2679–2699, https://doi.org/10.1007/BF02644569.
[3] M. Odnobokova, A. Belyakov, R. Kaibyshev, Grain refinement and strengthening of austenitic stainless steels during large strain cold rolling, Philos. Mag. A 99 (5) (2019) 531–556, https://doi.org/10.1080/14786435.2018.1546961.
[4] B. Maxwell, P.H. Rothschild, Cold working of polyethylene, J. Appl. Polym. Sci. 5 (16) (1961) S11–S13, https://doi.org/10.1002/app.1961.070051617.
[5] Y. Yang, J. Keum, Z. Zhou, G. Thompson, A. Hiltner, E. Baer, Structure and properties of biaxial-oriented crystalline polymers by solid-state crossrolling, J. Appl. Polym. Sci. 118 (2) (2010) 659–670, https://doi.org/10.1002/app.32414.
[6] S.J. Pan, H.R. Brown, A. Hiltner, E. Baer, Biaxial orientation of polypropylene by hydrostatic solid state extrusion. Part I: orientation mechanism and structural hierarchy, Polym. Eng. Sci. 26 (14) (1986) 997–1006, https://doi.org/10.1002/pen.760261406.
[7] A. Pawlak, A. Galeski, Plastic deformation of crystalline polymers: the role of cavitation and crystal plasticity, Macromolecules 38 (23) (2005) 9688–9697, https://doi.org/10.1021/ma050842o.
[8] D.M. Gezovich, P.H. Geil, Deformation of polyoxymethylene by rolling, J. Mater. Sci. 6 (1971) 509–530, https://doi.org/10.1007/BF00550306.
[9] R.M. McGlamery, Cold rolling film of high density ethylene polymer, U. S. Jpn. Outlook (April 2, 1963), 3083410.
[10] V. Beloshenko, Iu Vozniak, Y. Beygelzimer, Y. Estrin, R. Kulagin, Severe plastic deformation of polymers, Mater. Trans. 60 (7) (2019) 1192–1202.
[11] L.J. Broutman, R.S. Patil, Cold rolling of polymers. 1 influence of rolling on properties of amorphous polymer, Polym. Eng. Sci. 11 (2) (1971) 165–173, https://doi.org/10.1002/pen.760110212.
[12] H.E.H. Meijer, L.E. Govaert, Mechanical performance of polymer systems: the relation between structure and properties, Prog. Polym. Sci. 30 (8) (2005) 915–938, https://doi.org/10.1016/j.progpolymsci.2005.06.009.
[13] J. Snyder, A. Hiltner, E. Baer, Notch tip damage zone in biaxially oriented polypropylene at low temperature, J. Appl. Polym. Sci. 52 (2) (1994) 217–229, https://doi.org/10.1002/app.1994.070520209.
[14] S. Osawa, R. Porter, M. Ito, Uniplanar oriented isotactic polypropylene_3. Properties and morphology, Polymer 35 (3) (1994) 551–557.
[15] H.G.H. van Melick, L.E. Govaert, H.E.H. Meijer, Localisation phenomena in glassy polymers: influence of thermal and mechanical history, Polymer 44 (12) (2003) 3579–3591, https://doi.org/10.1016/S0032-3861(03)00089-2.
[16] Z. Bartczak, A.S. Argon, R.E. Cohen, Texture evolution in large strain simple shear deformation of high density polyethylene, Polymer 35 (16) (1994) 3427–3441, https://doi.org/10.1016/0032-3861(94)90905-9.
[17] Z. Barczak, R.E. Cohen, A.S. Argon, Evolution of the crystalline texture of high-density polyethylene during uniaxial compression, Macromolecules 25 (1992) 4692–4704.
[18] Z. Bartczak, A.S. Argon, R.E. Cohen, Morphological alterations during texture-producing plastic plane strain compression of high-density polyethylene, Macromolecules 25 (1992) 5705–5718.
[19] Z. Bartczak, Deformation of high-density polyethylene produced by rolling with side-constraints. I. Orientation Behavior, J. Appl. Polym. Sci. 86 (2002) 1396–1404, https://doi.org/10.1002/app.11284.
[20] D.P. Pope, A. Keller, Deformation of oriented polyethylene, J. Polym. Sci. Polym. Phys. Ed 13 (1975) 533–566.
[21] R. Hiss, S. Hobeika, C. Lynn, G. Stroble, Network stretching, slip processes, and fragmentation of crystallites during uniaxial drawing of polyethylene and related copolymers. A comparative study, Macromolecules 32 (13) (1999) 4390–4403.
[22] Z. Bartczak, Deformation of high-density polyethylene produced by rolling with side constraints. I. Orientation behavior, J. Appl. Polym. Sci. 86 (6) (2002) 1396–1404, https://doi.org/10.1002/app.11284.
[23] A. Pawlak, A. Rozanski, A. Galeski, Thermovision studies of plastic deformation and cavitation in polypropylene, Mech. Mater. 67 (2013) 104–118, https://doi.org/10.1016/j.mechmat.2013.07.016.
[24] S. Bahadur, The effect of hot and cold rolling on the properties of poly (oxymethylene), Polym. J. 7 (6) (1975) 613–621, https://doi.org/10.1295/polymj.7.613.
[25] D. Roylance, M. Roylance, Orientation profile in rolled polypropylene, J. Polym. Sci. B Polym. Lett. 10 (4) (1972) 273–277, https://doi.org/10.1002/pol.1972.110100408.
[26] O.B. Salamatina, S.N. Rudnev, Z. Bartczak, A. Galeski, E.F. Oleinik, Thermodynamics of inelastic deformation of amorphous and crystalline phases in linear polyethylene, Polym. Sci. 53 (9) (2011) 775–786, https://doi.org/10.1134/S0965545X11090100.
[27] F. Addiego, A. Dahoun, C. G'Sell, J.-M. Hiver, Characterization of volume strain at large deformation under uniaxial tension in high-density polyethylene, Polymer 47 (12) (2006) 4387–4399, https://doi.org/10.1016/j.polymer.2006.03.093.
[28] Z. Bartczak, A. Vozniak, WAXS/SAXS study of plastic deformation instabilities and lamellae fragmentation in polyethylene, Polymer 177 (2019) 160–177, https://doi.org/10.1016/j.polymer.2019.05.076.
[29] R. Pritchard, The transparency of crystalline polymers, Polym. Eng. Sci. 4 (1) (1964) 66–71, https://doi.org/10.1002/pen.760040114.
[30] R.S. Stein, M.B. Rhodes, Photographic light scattering by polyethylene films, J Appl Polym Phys 31 (11) (1960) 1873–1884, https://doi.org/10.1063/1.1735468.
[31] S. Bensason, J. Minick, A. Moet, S. Chum, A. Hiltner, E. Baer, Classification of homogeneous ethylene-octene copolymers based on comonomer content, J. Polym. Sci., Part B: Polym. Phys. 34 (7) (1996) 1301–1315, https://doi.org/10.1002/(SICI)1099-0488(199605)34:7<1301::AID-POLB12>3.0.CO;2-E.
[32] J.G. Williams, H. Ford, Mechanical properties of some cold-rolled plastics, J. Mech. Eng. Sci. 9 (5) (1967) 362–369, https://doi.org/10.1243/JMES_JOUR_1967_009_056_02.
[33] L.E. Nielsen, Models for the permeability of filled polymer systems, J. Macromol. Sci. A1 (5) (1967) 929–942, https://doi.org/10.1080/10601326708053745.
[34] S. Srinivas, P. Brant, Structure and properties of oriented polyethylene films, Polym. Eng. Sci. 43 (4) (2003) 831–849.
[35] K.E. Russell, B.K. Hunter, R.D. Heyding, Monoclinic polyethylene revisited, Polymer 38 (6) (1997) 1409–1414, https://doi.org/10.1016/S0032-3861(96)00643-X.
[36] M.E. Vickers, H. Fischer, Real-time *in situ* X-ray diffraction study of polyethylene deformation, Polymer 36 (13) (1995) 2667–2670, https://doi.org/10.1016/0032-3861(95)91216-T.

[37] G. Meinel, A. Peterlin, Plastic deformation of polyethylene IV. Rolling of polyethylene, Kolloid Z. Z. Polym. 242 (1970) 1151–1160, https://doi.org/10.1007/BF02084721.
[38] H.E.H. Meijer, L.E. Govaert, Mechanical performance of polymer systems: the relation between structure and properties, Prog. Polym. Sci. 30 (8) (2005) 915–938, https://doi.org/10.1016/j.progpolymsci.2005.06.009.
[39] T. Juska, I.R. Harrison, A criterion for craze formation, Polym. Eng. Sci. 22 (12) (1982) 766–776, https://doi.org/10.1002/pen.760221207.
[40] Y. Men, J. Rieger, G. Strobl, Role of the entangled amorphous network in tensile deformation of semicrystalline polymers, Phys. Rev. Lett. 91 (9) (2003), 095502, https://doi.org/10.1103/PhysRevLett.91.095502.

Update

Polymer
Volume 262, Issue , 2 December 2022, Page

DOI: https://doi.org/10.1016/j.polymer.2022.125508

Polymer 262 (2022) 125508

Contents lists available at ScienceDirect

Polymer

journal homepage: www.elsevier.com/locate/polymer

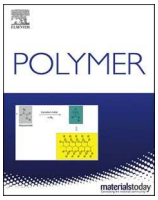

Corrigendum

Corrigendum to "Hierarchical solid-state structure and mechanical property relationships in cross-rolled polyethylene" [Polymer 254 (2022) 125039]

N. McMullen *, C. Zhang, C.F. Cheng, G.E. Wnek, A. Olah, E. Baer

Department of Macromolecular Science and Engineering, Case Western Reserve University, Cleveland, OH, 44106, USA

The authors regret the following unit errors in Sect. 3.7 of the published article:

1) "200 μm with a standard deviation of 50 μm" should be "200 nm with a standard deviation of 50 nm"

2) "270 μm with a standard deviation of 60 μm" should be "270 nm with a standard deviation of 60 nm"

The authors would like to apologise for any inconvenience caused.

DOI of original article: https://doi.org/10.1016/j.polymer.2022.125039.

* Corresponding author.
E-mail address: nam77@case.edu (N. McMullen).

https://doi.org/10.1016/j.polymer.2022.125508

Available online 14 November 2022